



Published in final edited form as:

*Proc SPIE Int Soc Opt Eng.* 2019 February ; 10953: . doi:10.1117/12.2513007.

## Methods for quantitative characterization of bone injury from computed-tomography images

Pablo Hernandez-Cerdan<sup>a</sup>, Beatriz Paniagua<sup>a</sup>, Jack Prothero<sup>b</sup>, J. S. Marron<sup>b</sup>, Eric Livingston<sup>c</sup>, Ted Bateman<sup>c</sup>, and Matthew McCormick<sup>a</sup>

<sup>a</sup>Kitware, Inc. 101 East Weaver Street, Carrboro, NC, USA 25710

<sup>b</sup>Dept. of Statistics and Operations Research, University of North Carolina at Chapel Hill, Hanes Hall, Campus Box 3260, Chapel Hill, NC, USA 27599

<sup>c</sup>Dept. of Biomedical Engineering, University of North Carolina at Chapel Hill, 4103 Thurston-Bowles Bldg, 104 Manning Dr. Campus Box 7575, Chapel Hill, NC, USA 27599

### Abstract

Computed tomography (CT) images can potentially provide insights into bone structure for diagnosis of disorders and diseases. However, evaluation of trabecular bone structure and whole bone shape is often qualitative or semi-quantitative. This limits inter-study comparisons and the ability to detect subtle bone quality variations during early disease onset or in response to new treatments. In this work, we enable quantitative characterization of bone diseases through bone morphometry, texture analysis, and shape analysis methods.

The potential of our analysis methods to identify the impact of hemophilia is validated in a mouse femur wound model. In our results, shape localizes and characterizes the formation of spurious bone, and our texture and bone morphometry analysis results provide extra information about the composition of that bone. Some of our one-dimensional (1D) textural features were able to significantly differentiate our injured femurs from our healthy femurs, even with this small sample size demonstrating the potential of the proposed analysis framework. While trabecular bone morphometrics have been a pillar in 3D microCT bone research for decades, the proposed analysis framework augments how we define and understand phenotypical presentation of bone disease. The contributed open source software is exposed to the medical image analysis community through 3D Slicer extensions to ensure both robustness and reproducibility.

## 1. INTRODUCTION

Bone diseases are common in the United States, especially among the elderly and individuals of low socioeconomic status, and they take a large toll on the Nation's overall health status. For the first time in 2012, the Centers for Disease Control and Prevention (CDC) reported that one-in-two adults (126.6 million total) were affected with a musculoskeletal disease, twice the rate of chronic heart and lung conditions.<sup>1, 2</sup> Fractures and osteoporosis are the biggest problems associated with bone disease; they are common,

costly, and can become a chronic burden on both individuals and society.<sup>3</sup> Musculoskeletal diseases represent \$213 billion in health care costs annually for treatment, care, and lost wages.<sup>4, 5</sup> The CDC also reports that muscle and bone diseases are more prevalent in low socioeconomic populations, due to their relationships with other comorbidities such as diabetes or obesity.<sup>6</sup>

Despite its increasing burden to our society, there is a paucity of drugs or therapies that to prevent or reverse bone damage. Currently, regenerative medicine, tissue engineering, and pharmacological therapies are being studied as therapeutic approaches for bone diseases. Preclinical testing plays a major role in this process, enabling powerful and clinically translatable methods to monitor disease progression and test candidate drugs. Even though invasive biomarkers are possible options for preclinical studies, imaging is an important key technology to accelerate therapeutic approaches because it is easily translated into the clinical setting.

Both clinical and pre-clinical researchers working on the discovery of therapeutic approaches to bone deterioration need effective, quantitative, robust and reproducible ways to measure the effect of those therapies in bone scans. From among the various diagnostic tests available, imaging-based diagnostics are among the most important method to measure bone quality. Imaging provides a fast, scalable and non-invasive way to examine bone structure. However, image-based evaluation is often performed qualitatively or semi-quantitative and with disparate analysis paradigms, which is not sufficient to perform robust comparisons between studies, nor to detect the subtle variations in bone quality during early disease onset.<sup>7-9</sup>

Hemophilia is a disorder caused by insufficient clotting factors. Patients with this disease experience recurrent joint bleeding, which ultimately leads cartilage<sup>10</sup> and bone<sup>11</sup> destruction, and results in a pathogenic process that resembles other degenerative musculoskeletal processes, such as osteoarthritis.<sup>12</sup>

In this work we present open source software tools to quantify musculoskeletal health from micro-computed tomography images of bone. These methods are evaluated on mouse femur wound model images obtained during a hemophilia study. Our bone analysis algorithms are developed as part of the Insight Toolkit<sup>13</sup> (ITK), and include trabecular bone morphometry, texture analysis, and shape analysis methods. Analysis methods developed in ITK are computationally efficient, they take advantage of ITK's fast neighborhood operators, and they re-use intermediate computations in order to minimize memory use. More importantly, ITK is open-source software that provides access to complex image analysis algorithms without any cost for biomedical researchers. This is crucial to ensure both the robustness and reproducibility of any scientific study.

The proposed solution provides enhanced quantitative characterization of hemophilia-induced bone pathology, when compared with bone morphometric biomarkers alone.

## 2. MATERIALS

We used three, twenty-two week old (skeletally mature), genetically modified, male mice for this study. In healthy individuals, the F8 gene provides instructions for making the protein coagulation factor VIII. Coagulation factors are a group of related proteins essential for the formation of blood clots. After injury, clots protect the body by sealing off damaged blood vessels and preventing further blood loss. Gene knockout (FVIII<sup>-/-</sup>) mice were used as a model for hemophilia in this study. These knockout mice have a pathogenic pathway that is similar to hemophilia, and they present bleeding-induced bone and joint damage. Each mouse was subjected to knee joint hemorrhage in the left limb by puncturing the joint capsule with a needle. The right limb served as the uninjured control.<sup>14</sup> Two weeks after injury simulation, the mice were euthanized. During the injury period, hemorrhage caused bone deterioration that we quantitatively characterized with the proposed methods. Hind limbs were scanned at 10 $\mu$ m resolution using microCT ( $\mu$ CT80; Scanco Medical AG, Brttisellen, Switzerland).

MicroCT analysis was performed on the trabecular bone at the proximal tibia only, inferior to the growth plate, which is a common skeletal site for image-based analysis.

## 3. METHODS

We have developed a pipeline (see figure 2) to segment bone tissue regions and quantify biomarkers within those regions. This paper presents an example of analysis of microCT images of a hemophilia mouse model, but common components of this pipeline can be adapted to target other modalities and pathologies.

The first step, whole femur segmentation, began with a fixed threshold in Hounsefield units to the microCT data in order extract all bony structures. Then, we performed morphological closing with a large kernel to remove the majority of trabecular latices visible in the scan. This was followed by separation of connected components of each bony structures in order to isolate the largest connected component (femur) was isolated. Finally, we used active contour evolution<sup>15</sup> to fill in all the internal structures in the femur.

After femur segmentation, the right anatomy was mirrored onto the left. Then, we performed registration to bring both models to the same coordinate frame via the iterative closest point (ICP) registration algorithm. The core of the algorithm matches each vertex on one surface with the closest surface point on the other. Then the transformation that modifies one surface to best match the other (in a least square sense) was applied. Proper convergence of the surfaces requires multiple iterations. After femur segmentation and registration our pipeline performed the computation of the following biomarkers:

### Shape Analysis:

Our analysis framework used Iterative Closest Points (ICP) to quantitatively analyze shape differences between left and right limbs. This shape analysis methodology can be performed in the absence of shape correspondence (models that have the same number of points). ICP

is performed by computing distances or 3D vectors from each vertex of the left (injured) 3D femur model to the right (unaffected) 3D femur model.

### **Texture Analysis:**

We incorporated two different texture quantification algorithms to provide a statistical description of the local texture of a 3D image.<sup>16</sup>

### **Co-occurrence textural features:**

The computation of co-occurrence features is based on the grey level co-occurrence matrix (GLCM)<sup>17</sup> computed for each pixels neighborhood. We computed eight different textural features from the GLCM: Energy, entropy, correlation, inverse difference moment (IDM), Contrast, Cluster Shade, Cluster Prominence and Haralick's Correlation.

### **Run length textural features:**

The computation of the run length features was based on the gray level run length matrix (GLRLM)<sup>18</sup> computed for each pixels neighborhood. A gray-level run is a set of consecutive, co-linear picture points having the same grey-level value. The length of the run is the number of picture points in the run. The GLRLM matrix describes the local textural structure of each pixels' neighborhood. We compute ten different textural features from the GLRLM: short run emphasis (SRE), long run emphasis (LRE), grey level non-uniformity (GLN), run length non-uniformity (RLN), low grey level run emphasis (LGRE), high grey level run emphasis (HGRE), short run low grey level emphasis (SRLGE), short run high grey level emphasis (SRHGE), long run low grey level emphasis (LRLGE) and long run high grey level emphasis (LRHGE). Each one of these features characterize a different aspect of the 3D textural appearance of an image, as described in previous publications.<sup>16, 19, 20</sup>

### **Bone Morphometry:**

Morphometry (or morphometrics) refers to the quantitative analysis of form, quantifying the size or the shape of the studied object. Bone morphometry has been typically performed on histopathology images. Histomorphometry consists of slicing planes of *ex-vivo* bone and execution of a succession of 2D morphometry analysis on the tissue slices, which destroys the tissue. Additionally, due to the 2D nature of the images, even though certain types of features such as bone volume fraction (BV/TV) and specific bone surface (BS/BV)<sup>21</sup> can be computed, computation of other 3D features, such as trabecular thickness (Tb.Th), trabecular separation (Tb.Sp), and trabecular number (Tb.N), is not possible.<sup>22</sup>

We computed five different traditional bone morphometry features: bone volume fraction (BV/TV), specific bone surface (BS/BV), trabecular thickness (Tb.Th), trabecular separation (Tb.Sp) and trabecular number (Tb.N).<sup>19, 23, 24</sup>

## 4. RESULTS

We analyzed the shape, texture, and morphometry on images from our hemophilia animal model. Our metrics were computed on the right unaffected limb and left (mirrored) limb, which experienced a bleeding-induced hemophilia-mimicking injury.

In our shape characterization, we observed that shaft volume in the left femur increased for all our cases. Our texture features and bone morphometrics provide additional information on the composition of bone growth that was induced as part of the pathological healing process.

Some one-dimensional (1D) textural features were able to significantly differentiate our injured femurs from healthy femurs, even with this small sample size. Those features are Short Run Emphasis ( $p=0.048$ ), entropy ( $p=0.036$ ), inertia ( $p=0.037$ ), Short Run Emphasis ( $p=0.048$ ) and Long Run Emphasis ( $p=0.034$ ). The rest of our 1D textural and bone morphometry features trended towards significance, suggesting that significance will be reached with a larger sample size. Our power analysis estimates many features will reach significance after an increase in the group sample size to 8 subjects. In addition to 1D features, our framework can compute 3D textural maps. Figure 3 presents results for one of the textural maps, the run length non-uniformity (RLN). RLN is a feature based on the run length texture analysis method.<sup>18</sup> RLN measures the similarity of the length of runs throughout the image. The RLN is expected to be small if the run-lengths are alike throughout the image. The RLN map shows and clearly quantifies newly formed highly-porous bone and non-dense bone within the subcortical plate. Figure 3 a) and b) shows corresponding locations in the right (a) and left (b) shafts and demonstrates distinct RLN in the subcortical plates of the left limb only (purple, high value areas). These textural maps are 3D and can be segmented to quantify the volume of pathology-induced tissue. We found a volumetric increase in elevated RLN in the injured limb: elevated RLN increased by 4.81% (20.38% volume of elevated RLN map values in the right limb compared to 25.19% in the left limb).

A principal component analysis (PCA) on the features, Figure 3 c), suggests that the first principal component could distinguish injured and unaffected limbs. Furthermore, the first principal component of the feature sets appear to coincide.

Figure 4 visualizes the result of our shape analysis. In all cases there are different degrees of bone deterioration in the anterior aspect of the left femur compared to the right. In many instances, a hematoma resulted from the joint puncture and influences the shape of new surface ossification. All left femurs also present spurious bone formation in the third trochanter, and bone enlargement in the lateral and medial shafts of the bone. Positive distances (red) in this distance map indicate injury-induced bone resorption, while negative distances indicate injury-induced bone apposition (blue). Despite joint puncture realized on the left limb, which does not impart direct damage to the bone, the anatomy is observed to change heavily adjacent to areas where blood pools.

## 5. CONCLUSIONS

In a previously published<sup>14</sup> study, Scanco analysis software was used to calculate trabecular bone volumetric density (BV/TV), trabecular connectivity density, trabecular number and thickness, bone tissue mineral density, and volumetric bone mineral density (vBMD) in 3D. We computed biomarkers based not only on traditional bone morphometrics, but also texture and shape-based metrics to obtain better statistical sensitivity to the impact of hemophilia on wound healing.

This work demonstrates that combining bone morphometrics, texture features, and shape characteristics have the potential to detect and quantify bone pathology. Open source applications to perform analysis are provided as 3D Slicer<sup>25</sup> extensions. A package containing 3D Slicer with all required extensions \* in addition to a dataset<sup>†</sup> is provided to reproduce the results presented in this work.

## REFERENCES

- [1]. Centers for Disease Control, “National Health Interview Survey (NHIS), Adult Sample,” (2012).
- [2]. Agency for Healthcare Research and Quality, U. D. o. H., Research, and Quality, “Medical Expenditures Panel Survey (MEPS), 2008–2011,” (2011).
- [3]. Office of the Surgeon General (US)., “The Surgeon General’s Report on Bone Health and Osteoporosis: What It Means to You,” (2015).
- [4]. NHAMCS\_OP, NHAMCS\_ED, N., “National Center for Health Studies, NHDS,” (2011).
- [5]. Agency for Healthcare Research and Quality, U. D. o. H., Research, and Quality, “Healthcare Cost and Utilization Project (HCUP).”
- [6]. Gheno R, Cepparo JM, Rosca CE, and Cotten A, “Musculoskeletal disorders in the elderly.,” *Journal of Clinical Imaging Science* 2, 39 (2012). [PubMed: 22919553]
- [7]. Bastick AN, Belo JN, Runhaar J, and Bierma-Zeinstra SMA, “What are the prognostic factors for radiographic progression of knee osteoarthritis?: A meta-analysis,” *Clin Orthop Relat Res* 473, 2969–2989 (9 2015). [PubMed: 25995176]
- [8]. Cooper C, Snow S, McAlindon TE, Kellingray S, Stuart B, Coggon D, and Dieppe PA, “Risk factors for the incidence and progression of radiographic knee osteoarthritis,” *Arthritis & Rheumatism* 43(5) (2000).
- [9]. Mazzuca SA, Brandt KD, Katz BP, Lane KA, and Buckwalter KA, “Comparison of quantitative and semiquantitative indicators of joint space narrowing in subjects with knee osteoarthritis,” *Ann Rheum Dis* 65, 64–68 (1 2006). [PubMed: 15919678]
- [10]. Hooiveld MJJ, Roosendaal G, Jacobs KMG, Vianen ME, van den Berg HM, Bijlsma JWJ, and Lafeber FPJG, “Initiation of degenerative joint damage by experimental bleeding combined with loading of the joint: A possible mechanism of hemophilic arthropathy,” *Arthritis & Rheumatism* 50, 2024–2031 (6 2004). [PubMed: 15188380]
- [11]. Sokoloff L, “Biochemical and physiological aspects of degenerative joint diseases with special reference to hemophilic arthropathy.,” *Annals of the New York Academy of Sciences* 240, 285–90 (1 1975). [PubMed: 1053873]
- [12]. Roosendaal G, van Rinsum AC, Vianen ME, van den Berg HM, Lafeber FP, and Bijlsma JW, “Haemophilic arthropathy resembles degenerative rather than inflammatory joint disease.,” *Histopathology* 34, 144–53 (2 1999). [PubMed: 10064394]

\* SPHARM-PDM, <https://www.nitrc.org/projects/spharm-pdm>, for shape analysis and BoneTexture, <https://www.slicer.org/wiki/Documentation/Nightly/Modules/BoneTexture>, for texture and bone morphometry.

† Dataset: <http://dx.doi.org/10.6084/m9.figshare.6947891>.

- [13]. Johnson HJ, McCormick M, Ibáñez L, and Consortium TIS, The ITK Software Guide. Kitware, Inc, third ed. (2013). In press.
- [14]. Lau AG, Sun J, Hannah WB, Livingston EW, Heymann D, Bateman TA, and Monahan PE, "Joint bleeding in factor VIII deficient mice causes an acute loss of trabecular bone and calcification of joint soft tissues which is prevented with aggressive factor replacement," *Haemophilia* 20, 716–722 (9 2014). [PubMed: 24712867]
- [15]. Zhu S, Lee T, and Yuille A, "Region competition: unifying snakes, region growing, energy/Bayes/MDL for multi-band image segmentation," in [Proceedings of IEEE International Conference on Computer Vision], 416–423, IEEE Comput. Soc. Press (1996).
- [16]. Vimort J. b., McCormick M, and Paniagua B, "Computing Bone Morphometric Feature Maps from 3-Dimensional Images," *Insight Journal* January-December 2017 (2017).
- [17]. Haralick RM, Shanmugam K, and Dinstein I, "Textural Features for Image Classification," *IEEE Transactions on Systems, Man, and Cybernetics* 3, 610–621 (11 1973).
- [18]. Galloway MM, "Texture analysis using gray level run lengths," *Computer Graphics and Image Processing* 4, 172–179 (6 1975).
- [19]. Vimort J.-b., McCormick M, Budin F, and Paniagua B, "Computing Textural Feature Maps for N-Dimensional images," *Insight Journal* 2017 January-December (2017).
- [20]. Vimort J-B, Ruellas A, Protrero J, Marron J, Shah H, Cevidanes L, Benavides E, and Paniagua B, "Detection of bone loss via subchondral bone analysis," in [Accepted to SPIE Medical Imaging], (2018).
- [21]. Jee WSS, "The past, present, and future of bone morphometry: its contribution to an improved understanding of bone biology.," *Journal of bone and mineral metabolism* 23 Suppl, 1–10 (2005).
- [22]. Voide R, van Lenthe GH, and Müller R, "Bone Morphometry Strongly Predicts Cortical Bone Stiffness and Strength, but Not Toughness, in Inbred Mouse Models of High and Low Bone Mass," *Journal of Bone and Mineral Research* 23, 1194–1203 (3 2008). [PubMed: 18348694]
- [23]. Hildebrand T, Laib A, Miller R, Dequeker J, and Regsegger P, "Direct three-dimensional morphometric analysis of human cancellous bone: Microstructural data from spine, femur, iliac crest, and calcaneus," *Journal of Bone and Mineral Research* 14(7), 1167–1174 (1999). [PubMed: 10404017]
- [24]. Bouxsein ML, Boyd SK, Christiansen BA, Guldberg RE, Jepsen KJ, and Miller R, "Guidelines for assessment of bone microstructure in rodents using microcomputed tomography," *Journal of Bone and Mineral Research* 25(7), 1468–1486 (2010). [PubMed: 20533309]
- [25]. Fedorov A, Beichel R, Kalpathy-Cramer J, Finet J, Fillion-Robin J-C, Pujol S, Bauer C, Jennings D, Fennessy F, Sonka M, Buatti J, Aylward S, Miller JV, Pieper S, and Kikinis R, "3d slicer as an image computing platform for the quantitative imaging network," *Magn Reson Imaging* 30, 1323–1341 (11 2012). [PubMed: 22770690]

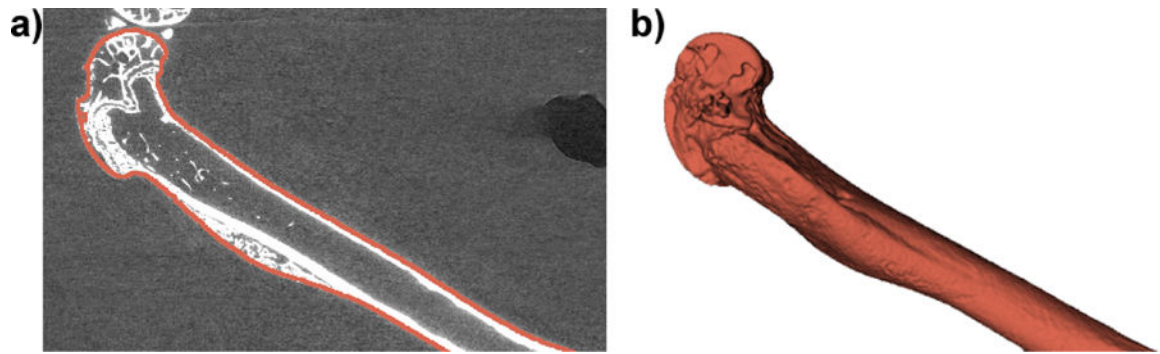


**Figure 1.**  
MicroCT data example. a) Grayscale with region of interest highlighted (femur) in red. b)  
3D rendering of the region of interest.

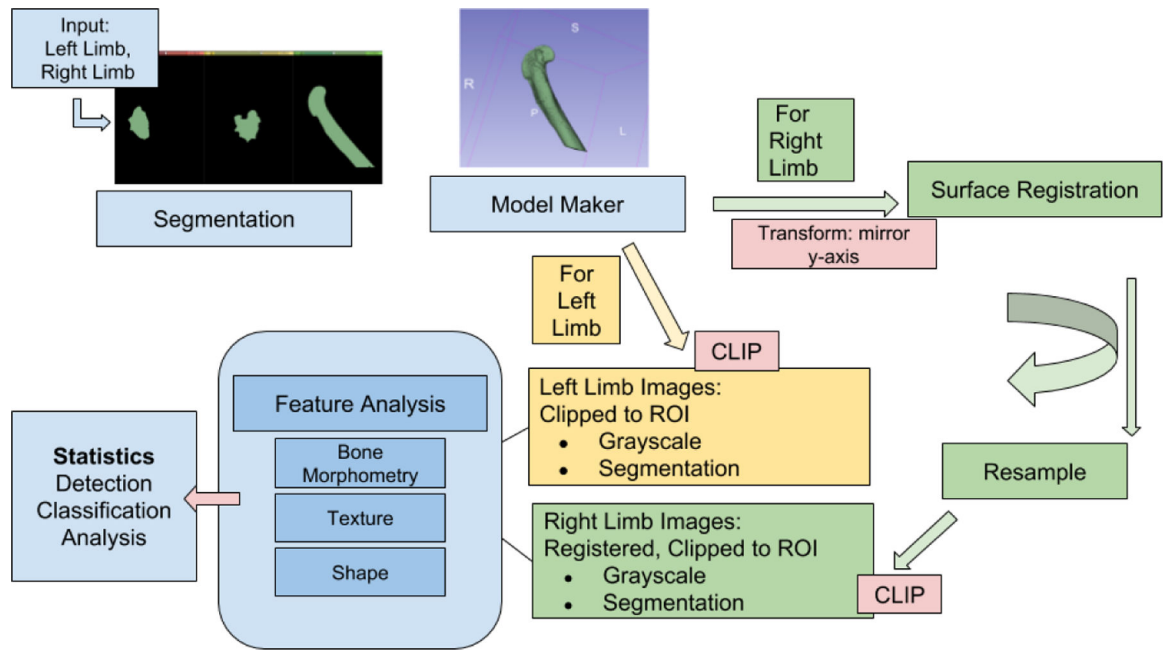


**Figure 2.**  
Workflow of the image analysis framework.

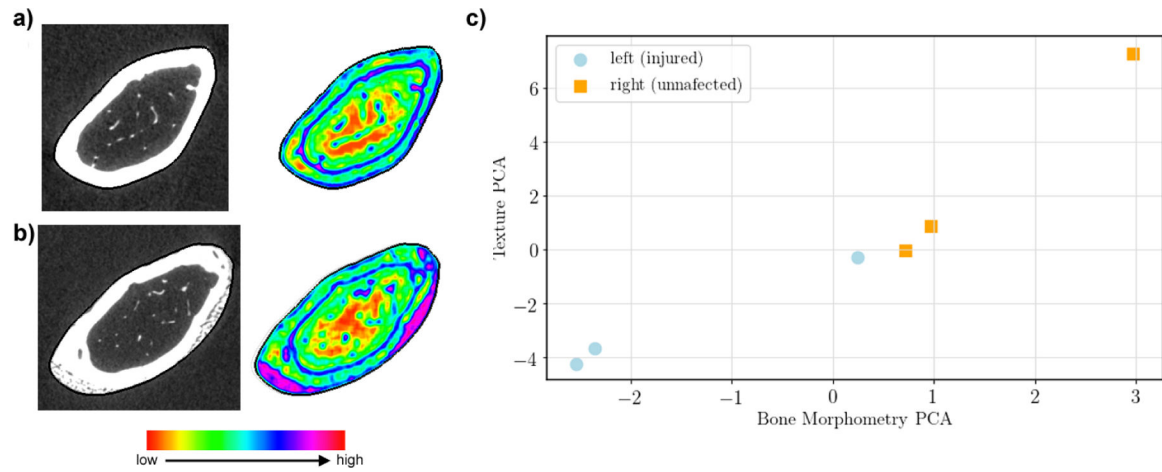


**Figure 3.** 3D texture maps and PCA of features. Run-length non-uniformity texture map for a) right (unaffected) femur, b) left (injured) femur. First column: microCT slice intensity. Second column: corresponding texture map (note that texture is computed on the 3D image, and that texture values in purple clearly identify injury-induced mass.). c) Plotting PCA first principal component of Bone Morphometry (5 features) against first principal component of texture analysis (18 features).

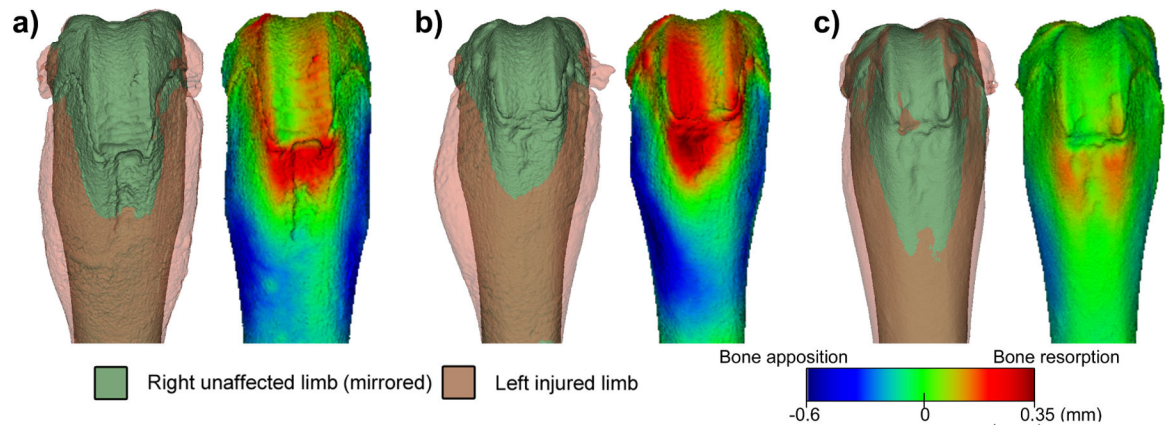


**Figure 4.** Shape analysis results for three subjects, including superimposed 3D models (left) and visualization of pathological shape changes via signed distances (right).